16th Australasian Fluid Mechanics Conference
Crown Plaza, Gold Coast, Australia
2-7 December 2007

The Influence of Spatial Resolution due to Hot-Wire Sensors on Measurements in Wall-Bounded Turbulence.

N. Hutchins[1], T. B. Nickels[2] and I. Marusic[1] M. S. Chong[1]

[1]Walter Bassett Aerodynamics Laboratory
Mechanical and Manufacturing Engineering
University of Melbourne, Victoria 3010 Australia.

[2]Department of Engineering
University of Cambridge, Cambridge CB2 1PZ UK.

Abstract

Reassessment of compiled data reveal that recorded scatter in the hot-wire measured near-wall peak in viscous-scaled streamwise turbulence intensity is due in large part to the simultaneous competing effects of Reynolds number and viscous-scaled wire-length l^+ ($= lU_\tau/\nu$, where l is the wirelength, U_τ is friction velocity and ν is kinematic viscosity). These competing factors can explain much of the disparity in existing literature, in particular explaining how previous studies have incorrectly concluded that the inner-scaled near-wall peak is independent of *Re*. We also investigate the appearance of the, so-called, 'outer-peak' in the broadband streamwise intensity, found by some researchers to occur within the log-region of high Reynolds number boundary layers. We show that this 'outer-peak' is most likely a symptom of attenuation of small-scales due to large l^+. Fully mapped energy spectra, obtained with two different l^+, are presented to demonstrate this phenomena. The spatial attenuation resulting from wires with large l^+ effectively filters small-scale fluctuations from the recorded signal.

Introduction

As a first approximation, the spatial attenuation due to a single-normal wire of finite spanwise length ought to be a simple case of integrating the fluctuating velocity across that span. For turbulent flows, this process is complicated by the fact that the velocity fluctuations are composed of a large range of superimposed time and length-scales. Boundary layers pose the additional complication that such fluctuations are anisotropic (owing to highly elongated turbulence structures) and are also a function of the distance from the wall. Thus for turbulent boundary layers it is unlikely that a treatment based purely on isotropic assumptions (such as that proposed by Wyngard [34]) will successfully describe attenuation due to spatial resolution. A successful analytical method must consider the width of the energetic fluctuations, as compared to the spanwise integral length of the sensor element. This requires spectral information in the spanwise direction (i.e. the energy contribution at each spanwise wavenumber, k_y). Direct Numerical Simulations (DNS) indicate that the spanwise spectral composition of u fluctuation is a highly complex function of distance from the wall (z) and Reynolds number *Re* (see for instance [1, 16]). Ultimately, as DNS are extended to ever higher Reynolds numbers, it may be possible to produce functional forms that describe this energy content for a given z and Reynolds number. However, until such time, we must continue to rely on experimental data to provide guidelines for spatial attenuation of hot-wire sensors.

Perhaps the most well-known experimental study into spatial resolution of hot-wire sensors is that performed by Ligrani & Bradshaw [19]. They interrogated a turbulent boundary layer at a single moderate Reynolds number, using numerous different sensors of varying l^+ and l/d. In so doing they produced two key recommendations for accurate measurements, both of which have since become standards for hot-wire design ($l^+ < 20$ and $l/d > 200$). Since that time, numerous other studies have attempted to consider the effects of spatial resolution, often with seemingly conflicting results. One problem here has been that few of these studies have repeated Ligrani & Bradshaw's approach of using numerous different hot-wire sensors at a single Reynolds number. Hence much of the spatial resolution behaviour is hidden within more subtle Reynolds number effects, as well as being spread across a wide number of (seemingly disparate) studies. We here attempt to redress this problem, following the insightful approach of Klewicki & Falco [18] to draw data together from a wide number of studies, considering simultaneously the effects of both Reynolds number and l^+.

As increasing numbers of higher Reynolds number experimental facilities come on-line, we would expect in general to see a tendency in experiments towards a relaxation of Ligrani & Bradshaw's key recommendations. Unless very large facilities are built, high Reynolds numbers will tend to be accompanied by a concurrent reduction in the viscous scale (i.e ν/U_τ will become small), making it increasingly difficult to ensure sensor lengths of $l^+ = 20$ or smaller. Thus there is a real need to expand our current knowledge of spatial resolution effects to higher Reynolds numbers. In addition, Ligrani and Bradshaw's investigation is focussed entirely on the near-wall region, close to the peak in streamwise turbulent intensity (at $z^+ \approx 15$, where z is the wall-normal ordinate and $z^+ = zU_\tau/\nu$). There is a real need to consider possible effects of spatial resolution on measurements in other regions of the boundary layer, particularly the log region where some recent high Reynolds number measurements seem to be reporting the existence of a second outer hump in the streamwise intensity [27, 8]. The existence of such an 'outer hump' is investigated here experimentally through the study of attenuation in energy spectra across a high Reynolds number ($Re_\tau = 14\,000$) boundary layer, using two wires of widely differing l^+.

Apparatus

Facility

Experiments are conducted in the High Reynolds Number Turbulent Boundary Layer Wind-Tunnel (HRNBLWT) at the University of Melbourne. This is an open-return blower wind-tunnel with working section nominally $27 \times 2 \times 1$ m. Measurements are made on the tunnel floor, 23 m downstream of the tripped inlet. Pressure gradient is nominally zero, with pressure coefficient (C_p) variation along the entire 27 m length set to within $\pm 1.0\%$. Further details of the facility are available in Nickels *et al.* 2005 & 2007 [28, 29].

Constant temperature anemometry

Re_τ	U_∞ (ms^{-1})	$\left(\frac{\nu}{U_\tau}\right)$ (μm)	δ (m)	probe	l (mm)	l^+	d (μm)	$\frac{l}{d}$	Δt^+	f_s (kHz)	f_{lp} (kHz)	$\left(\frac{TU_\infty}{\delta}\right)$
7350	9.84	44.9	0.330	55P05	1.00	22	5.0	200	0.37	20.000	10	14 600
7440	10.06	44.1	0.328	special	3.50	79	5.0	700	0.37	20.833	10	20 200
14210	19.94	23.0	0.326	55P15	0.50	22	2.5	200	0.70	40.000	20	22 000
14020	20.04	22.7	0.318	55P05	1.80	79	5.0	360	0.69	40.667	20	15 300

Table 1: Experimental parameters for hot-wire experiments.

All hot-wire probes are operated using an AA Lab Systems AN-1003 anemometer in constant temperature mode with overheat ratio of 1.8. The channels used for these measurements are all equipped with ultra low noise amplifier, frequency compensation and high performance signal conditioner. The measured frequency response of the system to an internal pulse was found in all cases to be greater than 50kHz. Fluctuating voltage signals from the anemometer were sampled using a 16 bit data acquisition board (Microstar DAP3000a/21). Sampling frequencies and low-pass filter settings are given in Table 1 along with sample intervals. The hot-wires are statically calibrated *in-situ* against a Pitot-static tube pair before and after each boundary layer traverse. Third-order polynomial curves are fitted to the calibration data to obtain calibration constants. Linear interpolation between the pre- and post-calibration curves is used to correct for temperature drift during the course of the experiment. Atmospheric conditions are monitored continuously throughout the experiments using a calibrated thermocouple and a barometer with an analogue output (Sensortechnics 144S-BARO). Freestream velocity U_∞ is also monitored throughout the course of the experiment using the calibration Pitot-static tube pair.

Probes

Two boundary layer type probe-body geometries are used through the course of these experiments; Dantec type 55P05 and 55P15 with prong spacings of 3 and 1.25 mm respectively. These probes are manufactured by the Auspex Corperation. The tungsten wires supplied by the vendor are removed and replaced with Wollaston wires (with a platinum core of various diameters d). The Wollaston wire is soldered to the prong tips and then etched over the central portion to reveal the desired length of platinum filament (l). See inset of Figure 1 for a sketch of the etched sensing element fabricated to a boundary type probe. For the majority of the data (except the very long probe lengths) this etched length is chosen to give an l/d ratio of 200 (where l is the length of the etched platinum filament and d is the diameter). This is in keeping with the earlier recommendations of Ligrani & Bradshaw [19]. For the very long wire lengths, a 55P05 probe body has been modified to give an overall prong spacing of 5 mm. This modified probe has higher length-to-diameter ratios (5 μm core with 3.5 mm etched length, giving an $l/d = 700$).

Experimental Conditions

Table 1 gives the full range of experimental conditions and probe/sensor geometries. Throughout the experiments described here, x, y and z are the streamwise, spanwise and wall-normal axes, with u, v and w denoting the respective fluctuating velocity components. U_∞ is the freestream velocity and U_τ is the friction velocity, determined from a Clauser fit to the logarithmic portion of the mean velocity data (using constants $\kappa = 0.41$ and $A = 5.0$). Capitalised velocities (e.g. U) and overbars indicate time-averaged values. The superscript $^+$ is used to denote viscous scaling of length (e.g. $z^+ = zU_\tau/\nu$) velocities (e.g. $U^+ = U/U_\tau$) and time (e.g. $t^+ = tU_\tau^2/\nu$). The friction Reynolds number Re_τ (also known as the Karman number or δ^+) is given by $\delta U_\tau/\nu$, where δ is the boundary layer thickness determined from a modified Coles law of the wall / wake fit to the mean velocity profile. The length of the platinum sensing element is given by l and l^+ in physical and viscous-scaled units respectively. The wire diameter is given by d and the length-to-diameter ratio by l/d. The sampling frequency and low-pass filter settings are denoted by f_s and f_{lp} respectively. The non-dimensional sample interval is given by $\Delta t^+ (= \Delta t U_\tau^2/\nu$, where $\Delta t = 1/f_s$). The total length in seconds of the velocity sample at each height is given by T. This is non-dimensionalised using outer variables to give sample length in terms of boundary layer turnover times TU_∞/δ. For converged statistics, these numbers need to be large. It is becoming clear that the largest structures in boundary layers, occurring in the logarithmic region, can commonly exceed 20δ in streamwise length [17, 12, 10, 9, 14, 26]. For converged statistics in the log region, we would typically require several hundreds of these events to advect past the sensor array (to ensure a stable enemble average). For facilities such as the Melbourne tunnel, where high Reynolds numbers are attained with relatively low flow speeds and a very long development length (to ensure a large viscous length-scale), such requirements can necessitate very lengthy boundary layer traverse experiments (approximately 12 hours for well converged statistics at $U_\infty = 10$ ms^{-1}).

The near-wall peak in streamwise turbulence intensity

Figure 1 shows a typical turbulence intensity and mean velocity profile from a hot-wire boundary layer traverse. It is noted that the turbulence intensity rises to a pronounced peak in the near-wall region. There is good general agreement over the wall-normal location of this peak, which appears to obey viscous scaling over a large range of Reynolds number, with $z_p^+ = 15 \pm 1$ widely reported in the literature (where the subscript p, refers to the peak value). Regarding the magnitude of the peak, however, there is more incongruity. We here denote the peak using the symbol φ such that,

$$\varphi = \left| \frac{\overline{u^2}}{U_\tau^2} \right|_p . \qquad (1)$$

This value is represented on Figure 1(a) by the horizontal dashed line. In a study that has since become a standard for hot-wire design, Ligrani & Bradshaw [19] unequivocally demonstrate that the measured value of φ is a function of the viscous-scaled length of the hot-wire sensing element (l^+), with φ tending to reduce as l^+ increases. The inset on Figure 1(a) includes a representation of the hot-wire sensor. The length l is defined as the length of the sensing element, which is the length of the etched (for Wollaston) or unplated (for tungsten type) portion of the wire. Whilst the results from [19] are compelling, the study was conducted at a single, quite low, Reynolds number ($Re_\tau \approx 1000$). In the interim, various studies have suggested

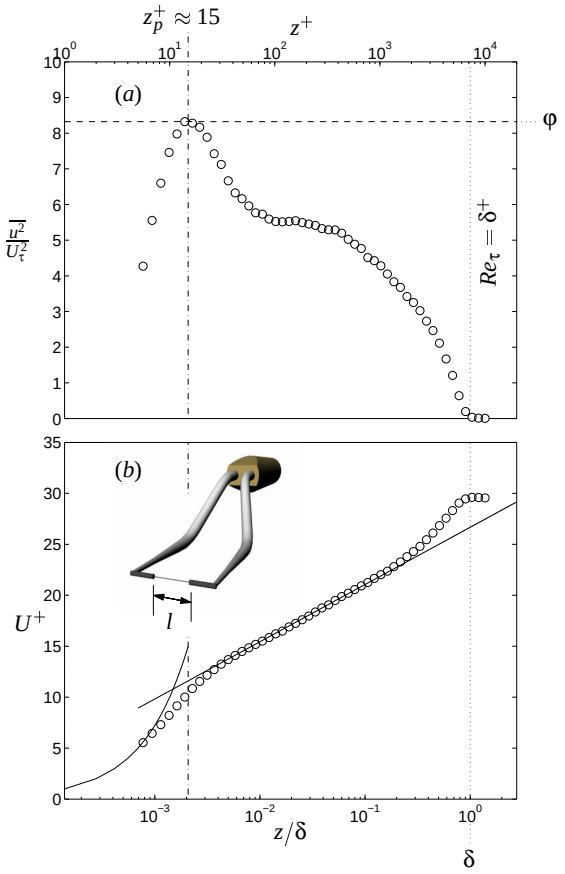

Figure 1: Example mean statistics from a turbulent boundary layer at $Re_\tau \approx 7300$ (*a*) turbulence intensity results, dashed horizontal line shows magnitude of peak intensity φ; (*b*) mean velocity profile, solid lines show linear and logartihmic regions, $u^+ = z^+$ and $u^+ = \frac{1}{\kappa}\log(z^+) + A$. Dotted lines show edge of boundary layer, and dot-dashed show wall-normal location of peak, z_p.

that the peak value φ may in fact also be a function of Reynolds number [18, 5, 23, 22, 21]. However, this assertion has not gone altogether unchallenged. Mochizuki & Nieuwstadt [24] and Durst *et al.* [6] have reported no growth in φ occuring with Reynolds number. In light of this controversy, we here approach this issue as a three parameter problem, attempting to quantify the peak intensity φ in a study where both l^+ and *Re* are varied. This set of measurements are summarized in Table 1. We also complement this data with a compendium of pre-existing results. For figure 2 we compile data for φ from numerous studies and plot these against given values of l^+ and Re_τ. The Karman number (or friction Reynolds number Re_τ) is a useful characterization of the flow in this instance since it provides a measure of the separation between outer and viscous scales, and hence is a true measure of scale separation. It is also equivalent to the boundary layer thickness expressed in viscous wall units (δ^+). A representation of Re_τ is included on Figure 1 as the vertical dotted line denoting the edge of the boundary layer.

The criteria for inclusion on Figure 2 are as follows. We sought out quality measurements in the literature (careful attention to facility, pressure gradient, freestream turbulence etc) made with single normal-wire hot-wire sensors where $l/d > 200$ (in order to isolate the effects of l/d, see Ligrani & Bradshaw [19]). Certain key data are not included. [1] The data used for the compilation are listed in the table below Figure 2. Since the data are not usually available in tabulated form, it is often necessary to take the value of φ from a figure (for which we use an in-house image mapping software). The value of l^+ and Re_τ are usually obtainable from tabulated experimental conditions, otherwise in the few cases where it is not possible to directly calculate Re_τ, we use an estimate of δ^+ based on the edge of the mean velocity profile such as the one shown in Figure 1(*b*). The presentation of the final compilation on a logarithmic *Re* axes will tend to be forgiving of any errors introduced by such estimates. This compilation is by no means exhaustive and we plan to continually update this database as and when new data become available or known to us.

Figure 2 shows this compiled data. Clearly when we just compare the peak intensity φ with Re_τ, as shown in plot (*a*), there is a large degree of scatter between studies. However, when the data are treated as a three-parameter problem, plotting φ against Re_τ and l^+ as shown in plot (*b*), the spread of data seem to lie rather well on a surface. The meshed plane shown in Figure 2(*b*) is a best-fit to all of the compiled data listed in the inset table, obtained by nonlinear least-squares regression fit to the form,

$$\varphi = A(l^+ \log_{10} Re_\tau) + B(l^+) + C(\log_{10} Re_\tau) + D, \qquad (2)$$

the best fit to which returns the following constants.

A	0.0161	B	-0.1079	C	1.2759	D	4.2699

The prescribed form of this fit is somewhat arbitrary, but at this stage it seems to provide a reasonable description of the available data. We would expect experimental scatter about this surface owing to other secondary effects that have not be accounted for, such as measurement error (which could be greater than $\pm 5\%$ especially if we consider error in determining U_τ), differences in facility design ('non-canonical' boundary layers due to pressure gradients, elevated freestream intensities, over/under-tripping etc) or the effects of temporal resolution (due to the finite temporal response of the anemometer/probe system).

Regardless, in simple terms, figure 2(*b*) and the fitted surface given by equation (2) show that the near-wall peak in turbulence intensity (φ) is subject to two primary competing effects. Whilst φ will tend to rise with Reynolds number, the measured value will drop with increasing l^+. As a preliminary attempt at fitting to limited scattered data, the surface given by equation (2) can explain some interesting trends in past results. If we rearrange equation 2 with respect to Re_τ, we can obtain an expression for the variation in l^+ necessary to yield a constant value of φ (which we here define as φ_c),

$$l^+ = \frac{\varphi_c - D - C\log_{10} Re_\tau}{A\log_{10} Re_\tau + B} \qquad (3)$$

For most facilities, if wire-length l is fixed this implies an approximately constant l/δ (fixed l/h and l/r for channels and pipes). Thus as an approximation we can state that l^+ increases approximately linearly with Re_τ.

$$l^+ = \frac{lU_\tau}{\nu} \approx \left(\frac{l}{\delta}\right)\frac{\delta U_\tau}{\nu} \approx \left(\frac{l}{\delta}\right) Re_\tau \qquad (4)$$

The forms taken by equations (3) & (4) are quite similar. Fig-

[1] The data of Ueda & Hinze [32], though oft cited, is not included due to insufficient l/d. The higher Reynolds number superpipe data of Morrison *et al.*[27] and the very short wires of Willmarth & Sharma [33] are discounted for similar reasons. We do not include those data of Österlund [30] which are listed as having $d = 1.27$ μm due to obvious inconsistencies in the results and the $d = 1.3$ μm data of Hites [11] is not included, due to the reported calibration drift.

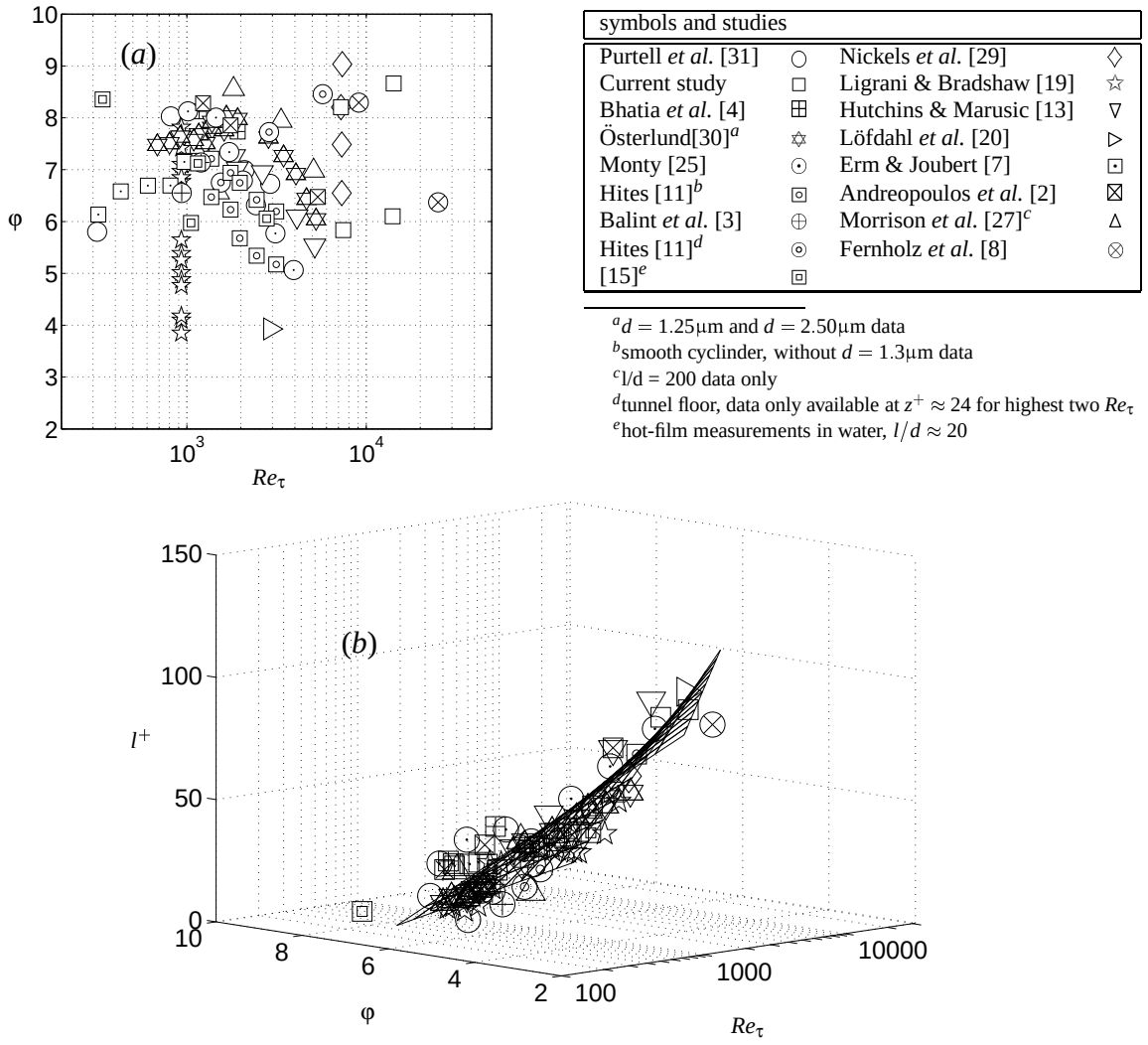

symbols and studies			
Purtell *et al.* [31]	○	Nickels *et al.* [29]	◇
Current study	□	Ligrani & Bradshaw [19]	☆
Bhatia *et al.* [4]	⊞	Hutchins & Marusic [13]	▽
Österlund[30][a]	✡	Löfdahl *et al.* [20]	▷
Monty [25]	⊙	Erm & Joubert [7]	⊡
Hites [11][b]	⊡	Andreopoulos *et al.* [2]	⊠
Balint *et al.* [3]	⊕	Morrison *et al.* [27][c]	△
Hites [11][d]	◎	Fernholz *et al.* [8]	⊗
[15][e]	⊡		

[a] $d = 1.25\mu$m and $d = 2.50\mu$m data
[b] smooth cyclinder, without $d = 1.3\mu$m data
[c] l/d = 200 data only
[d] tunnel floor, data only available at $z^+ \approx 24$ for highest two Re_τ
[e] hot-film measurements in water, $l/d \approx 20$

Figure 2: (*a*) Reynolds number variation of the peak measured value of the inner-scaled streamwise turbulence intensity (φ) for the various hot-wire experiments. Symbol legend and included studies are listed in the inset table; (*b*) Same data as three-dimensional plot against Re_τ and l^+. Meshed surface plane shows best-fit to the compiled data of the form given by equation 2.

ure 3 shows, as a dashed line, equation (4) evaluated for $(l/\delta) = 0.01$. The solid line shows equation (3) evaluated for $\varphi_c = 2.7^2$, which is the constant value of φ found by Mochizuki & Nieuwstadt [24], who compiled experimental boundary layer data and found no Reynolds number dependence for the peak value of streamwise turbulence intensity. The symbols plotted on Figure 3 show zero-pressure gradient experimental boundary layer data compiled by Mochizuki & Nieuwstadt [24]. It is clear that these symbols exhibit a general rise in l^+ as Reynolds number increases (since, in general, it is not possible to continually reduce the probe size as the viscous-scale reduces). This rise in l^+ approximately follows the trend predicted by equation 4 for an $(l/\delta) = 0.01$. (The most common wire diameter used in the literature is 5 μm which, if we assume an $l/d = 200$, gives a total $l = 1$ mm. Hence an (l/δ) of 0.01 implies an average boundary layer thickness $\delta \sim 100$ mm, which is certainly of the correct order for laboratory scale experiments.) It is also clear from the solid line on Figure 3 that this growth in l^+ with Reynolds number is very close to that required by equation 3 to return constant values of φ. Thus Figure 3 and equations (3) & (4) provide a very simple explanation of how past studies, such as those by Mochizuki & Nieuwstadt [24] and Durst *et al.* [6] have erroneously reported no dependance of peak streamwise intensity (φ) with Reynolds number. In short, φ will tend to increase with increasing Re_τ and reduce with increasing l^+. However, experimentally, a side-effect of increasing Re_τ is that l^+ is also, in general, increased. Thus, through sheer bad luck (assuming an $l/\delta \approx 100$ which it is shown, is a good approximation for most laboratory data), it is seen that experimental data can tend to fall on a region of the surface described by equation 2 that could give the misleading impression that φ is independent of Reynolds number.

The 'outer-hump' in broadband streamwise intensity: Is it real?

So far we have concentrated our attentions solely on the near-wall peak in streamwise turbulence intensity φ. However, attenuation due to spatial resolution also affects measurements away from the near-wall region. Figure 4 shows a comparison of two measurements made in a high Reynolds number turbulent boundary layer ($Re_\tau = 14\,000$) each with very different viscous-scaled wire-lengths ($l^+ = 22$ and 79). Figure 4(*a*) shows profiles of streamwise turbulence intensity. Measurements from the larger of the two wires (shown by the dashed lines) exhibit signs of attenuation out to beyond $z^+ = 300$. Not only has this attenuation depleted the near-wall peak (the approximate loca-

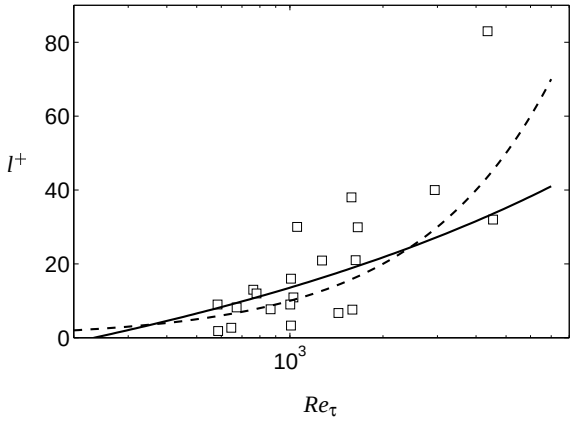

Figure 3: The rise in l^+ that tends to occur with Reynolds number (□) zero-pressure-gradient turbulent boundary layer data considered by Mochizuki & Nieuwstadt [24]. Dashed line shows (4) evaluated for $(l/\delta) = 0.01$. Solid line shows (3) evaluated at $\varphi_c = 2.7^2$.

tion of which is given by the left-hand vertical dashed line), but also appears to have uncovered a secondary peak, occurring in the log region of the boundary layer. Previous high Reynolds studies have also noted such secondary 'outer peaks' (Morrison *et al.* [27] & Fernholz *et al.* [8]). For Morrison *et al.* [27] the 'outer hump' has strongly emerged by $Re_\tau = 19\,700$, for which a wire with $l^+ = 76$ was employed. For Fernholz *et al.* [8], the 'outer hump' is clearly visible for their $Re_\tau = 25\,133$ data where $l^+ = 70$.

Closer analysis of the pre-multiplied energy spectra associated with each wall-normal location can explain the emergence of this peak. The plot shown in Figure 4(*b*) is formed by plotting iso-contours through the surface constructed from the one-dimensional pre-multiplied energy spectra of u fluctuations at each wall-normal z position. A more detailed explanation of how these energy maps are formed is given by Hutchins & Marusic [13, 14]. In these studies it was shown that, with high enough Reynolds numbers, the energy map has two clear energetic peaks. The peak closest to the wall has a location fixed in viscous wall-units (at $\lambda_x^+ = 1000$, $z^+ = 15$) and was termed the 'inner site', encompassing energetic contributions due to the near-wall cycle. The second peak occurs in the log region, with a location fixed in outer units (nominally reported at $\lambda_x = 6\delta$, $z/\delta \approx 0.05 - 0.06$), and was termed the 'outer' site. It was suggested [13] that this outer site might be the contribution due to the very long meandering features found to populate the log region (and termed 'superstructures'). The location of these two peaks are shown by the $+$ symbols on figure 4(*b*). Between these two peaks there is a region of inclined isocontours, where λ_x appears to scale with z, indicative of attached eddy type behaviour (the line $\lambda_x = 3z$ is included in red).

By comparing the two sets of contours, it is clear that the larger of the two wires ($l^+ = 79$, shown by the dashed contours) has attenuated the small-scale energy. This diminishes the 'inner site' and also the attached energy, leaving the 'outer site' as the increasingly dominant energetic contribution (this dominance of the large-scales will increase as l^+ becomes larger). Since the turbulence intensity shown in plot (*a*) is essentially the area under such contours, it is easy to see how attenuation due to spatial resolution can uncover a secondary 'outer hump' in the turbulence intensity profiles. Plots (*c*) and (*d*) show the premultiplied energy spectra at wall-normal locations corresponding to the inner and outer energetic sites respectively (shown by the vertical dotted lines on plots *a* and *b*). The wire with larger l^+ has depleted the inner energetic site (*a*) whilst, at sufficient Reynolds, number the 'outer energetic site' (*b*) is relatively unchanged. These results would strongly suggest that, rather than indicating some new phenomena of boundary layer turbulence, the 'outer humps' found by Morrison *et al.* [27] & Fernholz *et al.* [8] are more likely a symptom of wires with large l^+ spatially filtering small-scale fluctuations, which in turn will increasingly reveal the larger scale contribution due to the outer energetic site (the energetic contribution due to superstructures).

Effects of l^+ not confined to the near-wall

It is important to note that the effects of spatial resolution should not be considered to be confined merely to the near-wall region. Whilst the inner energetic site exhibits the most noticable attenuation, there is also significant attenuation throughout the attached regime, at least to $z^+ = 300$ for wires with $l^+ = 79$. Recent measurements with an $l^+ = 140$ wire (not shown here) indicate that for very long wires, this attenuation can extend to $z^+ = 1500$. Clearly we must be cautious when attempting to state wall-normal locations or wavelengths (λ_x) above which effects due to spatial resolution will be negligible. Based on a knowledge of the energy maps shown in figure 4(*b*) we would expect attenuation due to spatial resolution to be a complex function of z^+, l^+ and Re_τ (see Hutchins & Marusic [13, 14]). It is unlikely that so complex a function will lend itself to simple attempts at defining a height ($z_{\min}$) above which spatial resolution errors will be negligible. In the past such attempts have been made (usually attempting to describe $z_{\min}$ as a linear function of l^+).

Conclusions

The magnitude of the near-wall peak in inner-scaled broadband intensity φ is subject to the competing effects of Reynolds number and l^+. As Reynolds number is increased, there is an increasing presence of large-scale energy in the near-wall region (see [14, 13]), whilst the small-scale energy remains approximately the same. Thus, the net effect of increasing Re is an increase in the recorded value of φ. As l^+ is increased, on the other hand, the recorded small-scale fluctuation becomes increasingly attenuated (whilst the recorded large scales are effectively unmodified, see figure 4*d*). Thus the net effect of increasing l^+ is a reduction in the measured near-wall peak (φ). Consideration of these competing effects provides some explanation for the wide scatter exhibited by previous measurements of φ reported in the literature (see figure 2). When φ is plotted against l^+ and Re_τ, the available data seem to lie approximately within a common surface. A preliminary functional form is provided to describe this surface (2).

We show that the 'outer peak' in inner-scaled broadband intensity is most likely a symptom of spatial resolution issues. Certainly no outer-peak is present up to $Re_\tau = 14\,000$ for well-resolved turbulent intensity profiles made in the HRNBLWT facility. Only when the length of the wire is increased beyond $l^+ \approx 50 - 60$ do we begin to see signs of a secondary peak in the broadband intensity profile (not shown here, but see [29]). Analysis of fully mapped energy spectra (figure 4*b*) indicate that the larger wires attenuate the smaller-scale fluctuations. It is noted that these attenuated small-scales are not solely confined to the near-wall region, and extend throughout the log region in the form of attached eddies. Thus the effects of spatial resolution can extend a surprising distance from the wall. These far-reaching effects lead to the secondary peaks as noted by [27] and [8], which arise when the small-scale fluctuations are attenuated by the larger wires, to leave just the energetic contribution due to the very large scales that inhabit

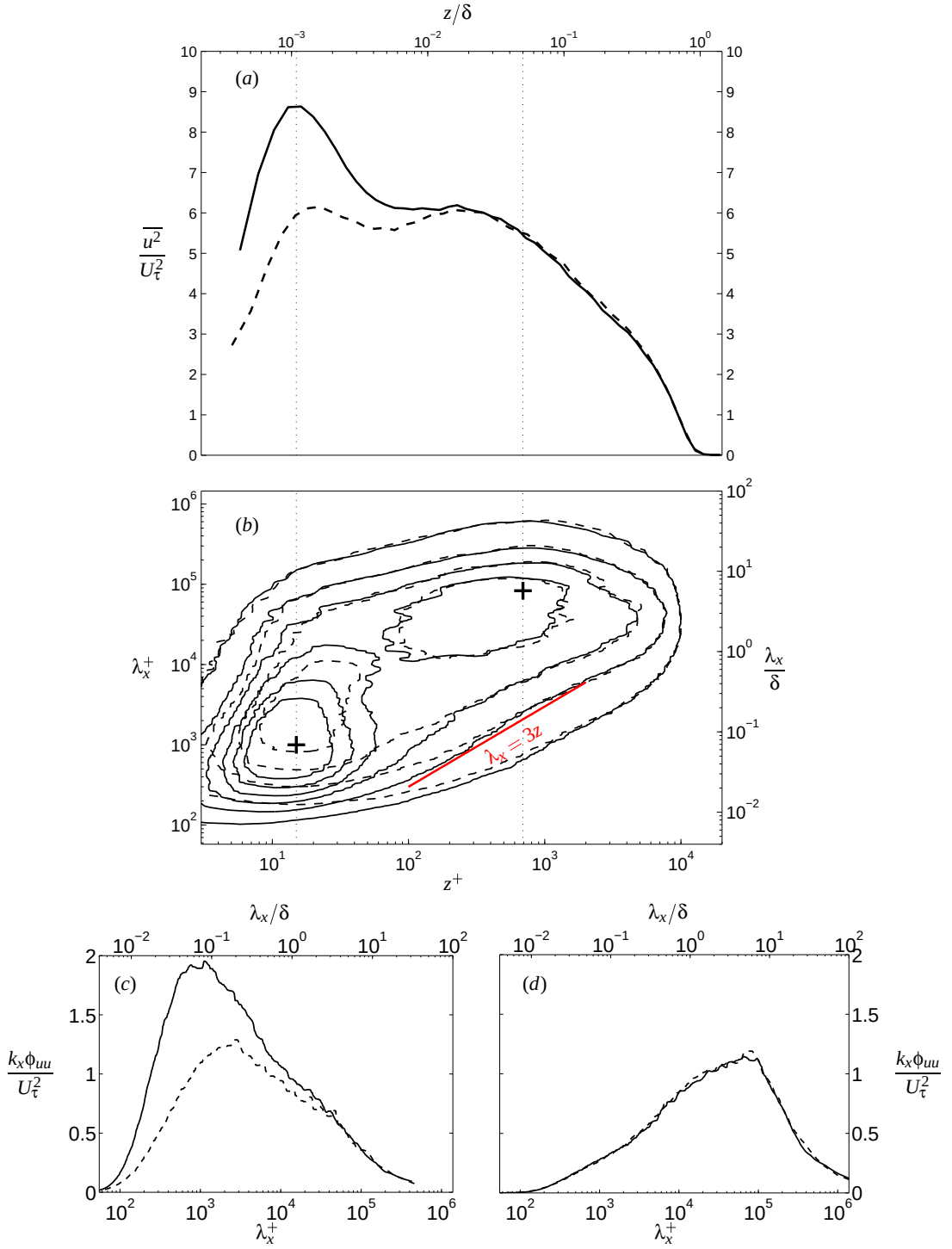

Figure 4: Comparison of two different wire lengths (solid) $l^+ = 22$; (dashed) $l^+ = 79$ at $Re_\tau \approx 14000$. (*a*) streamwise turbulence intensity profiles; (*b*) isocontours of premultiplied streamwise energy spectra $k_x\phi_{uu}$. Vertical dashed lines show $z^+ = 15$ and $z/\delta = 0.05$. Premultiplied energy spectra in these locations are given in plots (*c*) and (*d*) respectively.

the log region. The secondary peak in broadband intensity is effectively just the large-scale contribution in the log region, in the absence of the superimposed small-scale activity.

Acknowledgements

N.H and M.S.C wish to gratefully acknowledge the financial support of the Australian Research Council (DP-0663499). I.M acknowledges support from the Australian Research Council (Federation Fellowship FF0668703) and the David and Lucile Packard Foundation. T.B.N is grateful for support received from EPSRC.

References

[1] Abe, H., Kawamura, H. and Choi, H., Very large-scale structures and their effects on the wall shear-stress fluctuations in a turbulent channel flow up to $Re_\tau = 640$, *J. Fluids Eng.*, **126**, 2004, 835–843.

[2] Andreopoulos, J., Durst, F., Zaric, Z. and Jovanović, J., Influence of Reynolds number on characteristics of turbulent wall boundary layers, *Exp. Fluids*, **2**, 1984, 7–16.

[3] Balint, J.-L., Wallace, J. M. and Vukoslavčević, P., The velocity and vorticity vector fields of a turbulent boundary layer. Part 2. Statistical properties, *J. Fluid Mech.*, **228**, 1991, 53–86.

[4] Bhatia, J. C., Durst, F. and Jovanović, J., Corrections of hot-wire anemometer measurements near walls, *J. Fluid Mech.*, **122**, 1982, 411431.

[5] DeGraaff, D. B. and Eaton, J. K., Reynolds number scaling of the flat-plate turbulent boundary layer, *J. Fluid Mech.*, **422**, 2000, 319–346.

[6] Durst, F., Fischer, M., Jovanović, J. and Kikura, H., Methods to set up and investigate low Reynolds nuymber, fully developed turbulent plane channel flows, *J. Fluids Eng.*, **120**, 1998, 496–503.

[7] Erm, L. P. and Joubert, P. N., Low-reynolds-number turbulent boundary layers, *J. Fluid Mech.*, **230**, 1991, 144.

[8] Fernholz, H. H., Krausse, E., Nockermann, M. and Schober, M., Comparative measurementsin the canonical boundary layer at $Re_{\delta_2} \leqslant 6 \times 10^4$ on the wall of the German-Dutch windtunnel, *Phys. Fluids*, **7(6)**, 1995, 12751281.

[9] Ganapathisubramani, B., Clemens, N. T. and Dolling, D. S., Large-scale motions in a supersonic boundary layer, *J. Fluid Mech.*, **556**, 2006, 271–282.

[10] Guala, M., Hommema, S. E. and Adrian, R. J., Large-scale and very-large-scale motions in turbulent pipe flow, *J. Fluid Mech.*, **554**, 2006, 521–542.

[11] Hites, M. H., *Scaling of high-Reynolds number turbulent boundary layers in the National Diagnostic Facility*, Ph.D. thesis, Illinois Institute of Technology, Chicago, 1997.

[12] Hutchins, N., Ganapathisubramani, B. and Marusic, I., Dominant spanwise Fourier modes, and the existence of very large scale coherence in turbulent boundary layers, in *Proc. 15th Australasian Fluid Mech. Conf*, 2004, sydney.

[13] Hutchins, N. and Marusic, I., Evidence of very long meandering features in the logarithmic region of turbulent boundary layers, *J. Fluid Mech.*, **579**, 2007, 1–28.

[14] Hutchins, N. and Marusic, I., Large-scale influences in near-wall turbulence, *Proc. R. Soc. Lond.*, **365**, 2007, 647–664.

[15] Johansson, A. V. and Alfredsson, P. H., Effects of imperfect spatial resolution on measurements of wall-bounded turbulent shear flows, *J. Fluid Mech.*, **137**, 1983, 409421.

[16] Kasagi, K., Fukagata, K. and Suzuki, Y., Adaptive control of wall-turbulence for skin friction drag reduction and some consideration for high Reynolds number flows., in *2nd International Symposiumon Seawater Drag Reduction*, 2005, busan.

[17] Kim, K. C. and Adrian, R., Very large-scale motion in the outer layer, *Phys. Fluids*, **11**, 1999, 417–422.

[18] Klewicki, J. C. and Falco, R. E., On accurately measuring statistics associated with small-scale structure in turbulent boundary layers using hot-wire probes, *J. Fluid Mech.*, **219**, 1990, 119142.

[19] Ligrani, P. M. and Bradshaw, P., Spatial resolution and measurement of turbulence in the viscous sublayer sublayer using subminiature hot-wire probes, *Exp. Fluids*, **5**, 1987, 407–417.

[20] Löfdahl, L., Stemme, G. and Johansson, B., A sensor based on silicon technology for turbulence measurements, *J. Phys. E. Sci. Instrum.*, **22**, 1989, 391–393.

[21] Marusic, I. and Kunkel, G. J., Streamwise turbulence intensity formulation for flat-plate boundary layers, *Phys. Fluids*, **15**, 2003, 2461–2464.

[22] Metzger, M. M. and Klewicki, J. C., A comparative study of near-wall turbulence in high and low Reynolds number boundary layers, *Phys. Fluids*, **13**.

[23] Metzger, M. M., Klewicki, J. C., Bradshaw, K. L. and Sadr, R., Scaling the near-wall axial turbulent stress in the zero pressure gradient boundary layer, *Phys. Fluids*, **13, 6**, 2001, 1819–1821.

[24] Mochizuki, S. and Nieuwstadt, F. T. M., Reynolds-number-dependence of the maximum in the streamwise velocity fluctuations in wall turbulence, *Exp. Fluids*, **21**, 1996, 218–226.

[25] Monty, J. P., *Developments in smooth wall turbulent duct flow*, Ph.D. thesis, University of Melbourne, Australia, 2005.

[26] Monty, J. P., Stewart, J. A., Williams, R. C. and Chong, M. S., Large-scale features in turbulent pipe and channel flows, *J. Fluid Mech.*, in press.

[27] Morrison, J. F., McKeon, B. J., Jiang, W. and Smits, A. J., Scaling of the streamwise velocity component in turbulent pipe flow, *J. Fluid Mech.*, **508**, 2004, 99–131.

[28] Nickels, T. B., Marusic, I., Hafez, S. and Chong, M. S., Evidence of the k_1^{-1} law in a high-Reynolds-number turbulent boundary layer, *Phys. Rev. Letters*, **95**, 2005, 074501.

[29] Nickels, T. B., Marusic, I., Hafez, S., Hutchins, N. and Chong, M. S., Some predictions of the attached eddy model for a high Reynolds number boundary layer, *Proc. R. Soc. Lond.*, **365**, 2007, 807–822.

[30] Österlund, J. M., *Experimental studies of zero pressure-gradient turbulent boundary-layer flow*, Ph.D. thesis, Department of Mechanics, Royal Institute of Technology, Stockholm, 1999.

[31] Purtell, P., Klebanoff, P. and Buckley, F., Turbulent boundary layer at low Reynolds number, *Phys. Fluids*, **24**, 1981, 802–811.

[32] Ueda, H. and Hinze, J. O., Fine-structure turbulence in the wall region of a turbulent boundary layer, *J. Fluid Mech.*, **67**, 1975, 125–143.

[33] Willmarth, W. W. and Sharma, L. K., Study of turbulent structure with hot wires smaller that the viscous length, *J. Fluid Mech.*, **142**, 1984, 121–149.

[34] Wyngaard, J. C., Measurement of small-scale turbulence structure with hot-wires, *J. Phys. E.*, **1**, 1968, 1105–1108.